Original Article | Thoracic Imaging

eISSN 2005-8330
https://doi.org/10.3348/kjr.2020.0132
Korean J Radiol 2020;21(4):494-500

Korean Journal of Radiology
KJR

Chest Radiographic and CT Findings of the 2019 Novel Coronavirus Disease (COVID-19): Analysis of Nine Patients Treated in Korea

Soon Ho Yoon, MD, PhD[1], Kyung Hee Lee, MD, PhD[2], Jin Yong Kim, MD, MSc[3], Young Kyung Lee, MD, PhD[4], Hongseok Ko, MD[5], Ki Hwan Kim, MD[6], Chang Min Park, MD, PhD[1], Yun-Hyeon Kim, MD, PhD[7]

[1]Department of Radiology, Seoul National University College of Medicine, Seoul National University Hospital, Seoul, Korea; [2]Department of Radiology, Seoul National University Bundang Hospital, Seongnam, Korea; [3]Department of Internal Medicine, Incheon Medical Center, Incheon, Korea; [4]Department of Radiology, Seoul Medical Center, Seoul, Korea; [5]Department of Radiology, National Medical Center, Seoul, Korea; [6]Department of Radiology, Myongji Hospital, Goyang, Korea; [7]Department of Radiology, Chonnam National University Hospital, Gwangju, Korea

Objective: This study presents a preliminary report on the chest radiographic and computed tomography (CT) findings of the 2019 novel coronavirus disease (COVID-19) pneumonia in Korea.

Materials and Methods: As part of a multi-institutional collaboration coordinated by the Korean Society of Thoracic Radiology, we collected nine patients with COVID-19 infections who had undergone chest radiography and CT scans. We analyzed the radiographic and CT findings of COVID-19 pneumonia at baseline. Fisher's exact test was used to compare CT findings depending on the shape of pulmonary lesions.

Results: Three of the nine patients (33.3%) had parenchymal abnormalities detected by chest radiography, and most of the abnormalities were peripheral consolidations. Chest CT images showed bilateral involvement in eight of the nine patients, and a unilobar reversed halo sign in the other patient. In total, 77 pulmonary lesions were found, including patchy lesions (39%), large confluent lesions (13%), and small nodular lesions (48%). The peripheral and posterior lung fields were involved in 78% and 67% of the lesions, respectively. The lesions were typically ill-defined and were composed of mixed ground-glass opacities and consolidation or pure ground-glass opacities. Patchy to confluent lesions were primarily distributed in the lower lobes (p = 0.040) and along the pleura (p < 0.001), whereas nodular lesions were primarily distributed along the bronchovascular bundles (p = 0.006).

Conclusion: COVID-19 pneumonia in Korea primarily manifested as pure to mixed ground-glass opacities with a patchy to confluent or nodular shape in the bilateral peripheral posterior lungs. A considerable proportion of patients with COVID-19 pneumonia had normal chest radiographs.

Keywords: *Coronavirus; Pneumonia; COVID-19; Chest X-ray; Computed tomography*

INTRODUCTION

An outbreak of pneumonia of unknown etiology occurred in Wuhan, China in December 2019. A prompt investigation confirmed that the 2019 novel coronavirus disease (COVID-19; temporarily termed as 2019-nCoV) was responsible (1). Human-to-human transmission of COVID-19 was confirmed to be possible (2), and COVID-19 rapidly spread throughout China and to other countries. As of February 16, 2020, COVID-19 infections had been confirmed in 51857 patients globally, including 51174 patients in China and 683 patients outside China (3). The first

Received February 17, 2020; accepted after revision February 18, 2020.
This study was supported by the Korean Society of Thoracic Radiology.
Corresponding author: Soon Ho Yoon, MD, PhD, Department of Radiology, Seoul National University College of Medicine, Seoul National University Hospital, 101 Daehak-ro, Jongno-gu, Seoul 03080, Korea.
• Tel: (822) 2072-2584 • Fax: (822) 743-6385 • E-mail: yshoka@gmail.com

Korean Journal of Radiology
KJR

COVID-19 patient was identified in South Korea (hereafter, Korea) on January 20, 2020. As of February 16, there were 29 COVID-19 patients in Korea, placing Korea in fifth place internationally in terms of the number of COVID-19 patients, after China, Singapore (72 patients), Japan (53 patients), and Thailand (34 patients). Deaths have almost exclusively occurred in China (1666 patients; 3.3%), rather than outside China (3 patients; 0.4%). The discrepancy in the death rate between China and other countries might be due to differences in the disease manifestation of COVID-19 pneumonia or in other countries' capacity to manage a limited number of cases, in contrast to the overwhelming numbers of cases in China.

Early radiologic investigations consistently reported that the typical computed tomography (CT) findings of COVID-19 pneumonia were bilateral ground-glass opacities (GGOs) and consolidation with a peripheral and posterior lung distribution (4-6). The current publications on this topic are exclusively from China, and it remains unknown how COVID-19 pneumonia appears on chest radiographs and CT images of patients outside China. Therefore, we present a preliminary report on the chest radiographic and CT findings of COVID-19 pneumonia in Korea.

MATERIALS AND METHODS

This retrospective study was approved by the Institutional Review Board of the participating hospitals, and the requirement for informed consent was waived.

Patients

On February 6, 2020, the Korean Society of Thoracic Radiology proposed a multi-institutional collaboration for reporting the radiologic findings of COVID-19. Seven members with different affiliations decided to participate in this study, and the working group submitted a document for review by the Institutional Review Board of each affiliated hospital. Due to between-hospital differences in the required period for Institutional Review Board review, we expedited the process to report cases for which approval was received, while excluding cases under review. Consequently, we included nine consecutive patients (median age, 54 years; four men and five women) with COVID-19 infections confirmed through a pan-coronavirus conventional polymerase chain reaction assay from January 2020 through February 9, 2020 from Incheon Medical Center (7), Seoul National University Hospital, and Seoul National University Bundang Hospital.

CT Protocol

All CT examinations were performed using a multi-detector CT scanner with 64 or more channels (Somatom Definition, Somatom Definition AS+, or Somatom Force, Siemens Healthineers, Erlangen, Germany). The detailed parameters for CT acquisition were as follows: tube voltage, 120 kVp; tube current, standard (reference mAs, 60–120) to low-dose (reference mAs, 30) with automatic exposure control; slice thickness, 1.0 mm; reconstruction interval, 1.0–3.0 mm; and a sharp reconstruction kernel. CT images were obtained with the patient in the supine position at full inspiration and without contrast medium.

All patients underwent a baseline digital anteroposterior chest radiography at full inspiration using a mobile chest radiograph machine (FLUOROSPOT Compact FD, Siemens Healthineers; DRX-Revolution Mobile X-ray System, Carestream Health, Rochester, NY, USA; or Optima XR220, GE Healthcare, Milwaukee, WI, USA).

Eight of the nine patients had parenchymal abnormalities on their baseline chest CT scans. In another patient, the baseline chest CT scan was normal, and parenchymal abnormalities were observed on a follow-up CT scan one week later. Accordingly, we analyzed eight baseline chest CT scans and one follow-up CT scan with abnormal findings of COVID-19 pneumonia.

Image Analysis

Two attending radiologists (with 15 and 12 years of experience in chest imaging, respectively) reviewed the chest radiographs and CT images by consensus on a picture archiving and communication system (PACS, INFINITT Healthcare co., Ltd., Seoul, Korea). The readers assessed the presence, location, and density of parenchymal abnormalities on chest radiographs without reviewing the CT images, and graded the abnormalities using the following 5-point scale (8): 1, normal; 2, patchy atelectasis and/or hyperinflation and/or bronchial wall thickening; 3, focal alveolar consolidation involving no more than one segment or one lobe; 4, multifocal consolidation; and 5, diffuse alveolar consolidation. After the initial assessment of the chest radiographs, we checked whether the abnormalities on chest radiographs corresponded to abnormalities on chest CT images.

The CT images were evaluated with both lung (width, 1500 HU; level, -600 HU) and mediastinal (width, 400

 https://doi.org/10.3348/kjr.2020.0132

HU; level, 40 HU) window settings. The readers identified all separate pulmonary lesions on CT and analyzed the longest diameter, location, shape, density, and margin of the lesions. The locations of the lesions were specified as lobar, axial, and anteroposterior. For the axial location, the peripheral lung was defined as the outer one-third of the lung, and the central lung was defined as the inner two-thirds of the lung. According to a horizontal line dividing the lung into anterior and posterior halves, locations were classified as anterior or posterior. The shapes of the lesions were first categorized as patchy, confluent, or nodular. Patchy lesions were defined as isolated focal lesions with no nodular shape in the segment, and confluent lesions were defined as large fused lesions involving multiple segments. The densities of the patchy to confluent lesions were classified as pure GGO, mixed GGO and consolidation, consolidation, or a crazy-paving appearance. The densities of the nodular lesions were classified as pure GGO, part-solid, or solid. The margins of the lesions were dichotomized as ill-defined or well-defined. We evaluated whether the pulmonary lesions had a predilection for the lower lobes, pleura, or bronchovascular bundles. Furthermore, the readers evaluated the presence of air-bronchograms, the reversed halo sign, cavities, micronodules, a tree-in-bud appearance, and pleural effusion based on the Fleischner Society glossary of terms for thoracic imaging (9).

Statistical Analysis

Fisher's exact test was used to compare patchy to confluent lesions and nodular lesions in terms of the proportion of pure GGO lesions, axial location, anteroposterior location, margin, and predilection for the lower lobes, pleura, and bronchovascular bundles. Statistical analyses were performed using SPSS version 25.0 (IBM Corp., Armonk, NY, USA). *P* values < 0.05 were considered to indicate a statistically significant difference.

RESULTS

Baseline Chest Radiographic Findings

Five of the nine patients showed radiographic abnormalities (severity grade 2, one patient; grade 3, two patients; and grades 4 and 5, one patient each). Chest CT scans revealed that the grade 2 lesion and one of the grade 3 lesions as areas of prominent breast tissue mimicking faint GGO and post-inflammatory focal atelectasis on chest radiography, respectively. In summary, three of the nine patients (33.3%) were confirmed to have parenchymal abnormalities related to COVID-19 pneumonia on chest radiographs (Figs. 1A, 2A, 3A).

One of the three patients had a single nodular opacity in the left lower lung zone (Fig. 3A), and the other two patients had four and five patchy opacities in both lungs (Figs. 1A, 2A), respectively (Table 1). In a per-lesion analysis, 50% of the 10 opacities presented in the lower lung zones, 80% of the opacities were located in the peripheral lungs, and 70% of the opacities were areas of consolidation.

Chest CT Findings

In total, 77 lung parenchymal lesions were identified in the nine patients, of whom eight had bilateral

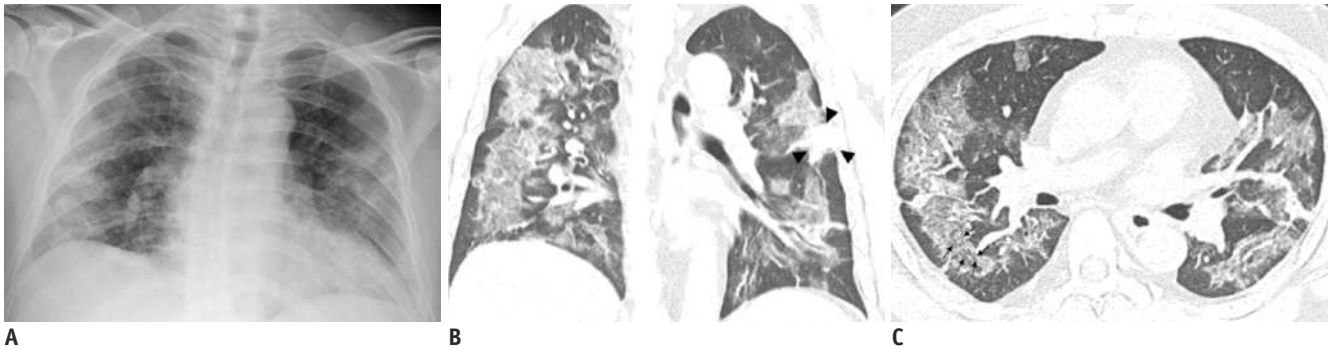

Fig. 1. Representative chest radiographic (A) and CT images (B, C) of COVID-19 pneumonia manifesting as confluent mixed ground-glass opacities and consolidation on CT. A. Anteroposterior chest radiograph shows multifocal patchy peripheral consolidations in bilateral lungs, except for left upper lung zone. **B, C.** Coronal and axial chest CT images show confluent mixed ground-glass opacities and consolidative lesions in peripheral bilateral lungs. Discrete patchy consolidation (arrowheads) is noted in left upper lobe. On axial CT image **(C)**, confluent lesions are mainly distributed in peripheral lung along bronchovascular bundles. Most of lesions spare juxtapleural area, and minor proportion of lesions touch pleura. Lesions contain multiple air-bronchograms, and air-bronchogram in superior segment of right lower lobe is distorted (arrows). COVID-19 = Coronavirus disease 2019, CT = computed tomography

https://doi.org/10.3348/kjr.2020.0132

Korean Journal of Radiology
KJR

lung parenchymal abnormalities. The median numbers of parenchymal lesions and involved lobes were 5 (interquartile range, 2–13) and 2 (interquartile range, 2–5), respectively. The most frequently involved lobe was the right lower lobe (eight patients), followed by the left upper and lower lobes (six patients each). Among the 77 identified lesions, 39% were patchy, 13% were confluent, and 48% were nodular (Table 2). The average diameters of the patchy, confluent, and nodular lesions were 2.6 ± 1.5 cm, 9.8 ± 2.6 cm, and 1.3 ± 0.6 cm, respectively. The peripheral and posterior lung were involved in 78% and 67% of the lesions, respectively. Patchy to confluent lesions were more prevalent than nodular lesions per patient (median relative proportion of patchy to confluent lesions, 86% [interquartile range, 33–100%]).

Patchy to confluent lesions primarily manifested as mixed GGO and consolidative lesions (50%) (Fig. 1B, C), followed by pure GGO lesions (35%) (Fig. 2B, C), lesions with a crazy-paving appearance (10%), and areas of consolidation (5%). The most frequent shape of the lesions was wedge-shaped (42%), followed by elongated (33%) and confluent (25%). They frequently had an ill-defined margin (70%) and

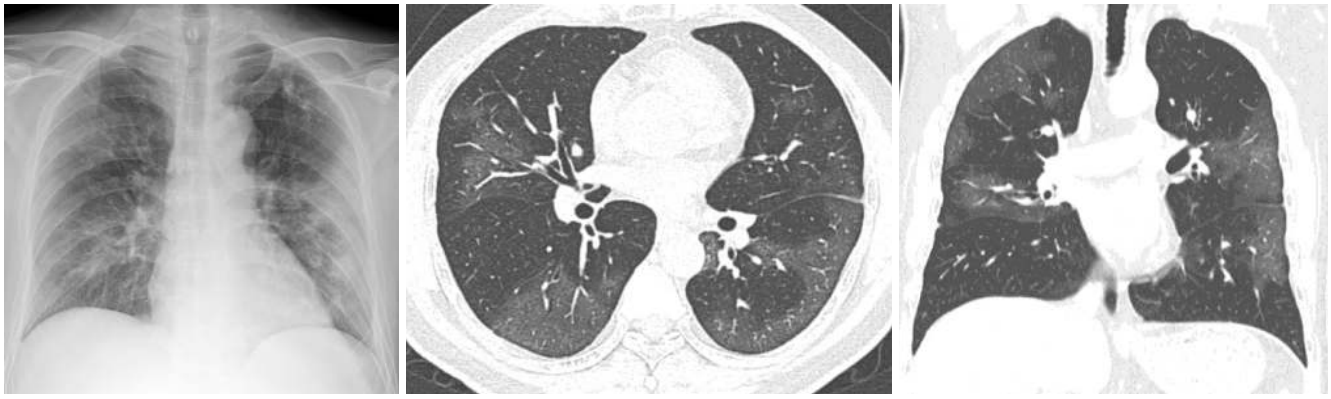

Fig. 2. Representative chest radiographic (A) and CT images (B, C) of COVID-19 pneumonia manifesting as confluent pure ground-glass opacities on CT. A. Baseline anteroposterior chest radiograph shows patchy ground-glass opacities in right upper and lower lung zones and patchy consolidation in left middle to lower lung zones. Several calcified granulomas are incidentally noted in left upper lung zone. **B, C.** Baseline axial and coronal chest CT images show confluent pure ground-glass opacities involving both lungs. Most of confluent and patchy ground-glass opacities about pleura and fissure in peripheral lung. A few calcified granulomas are incidentally noted in left upper lobe.

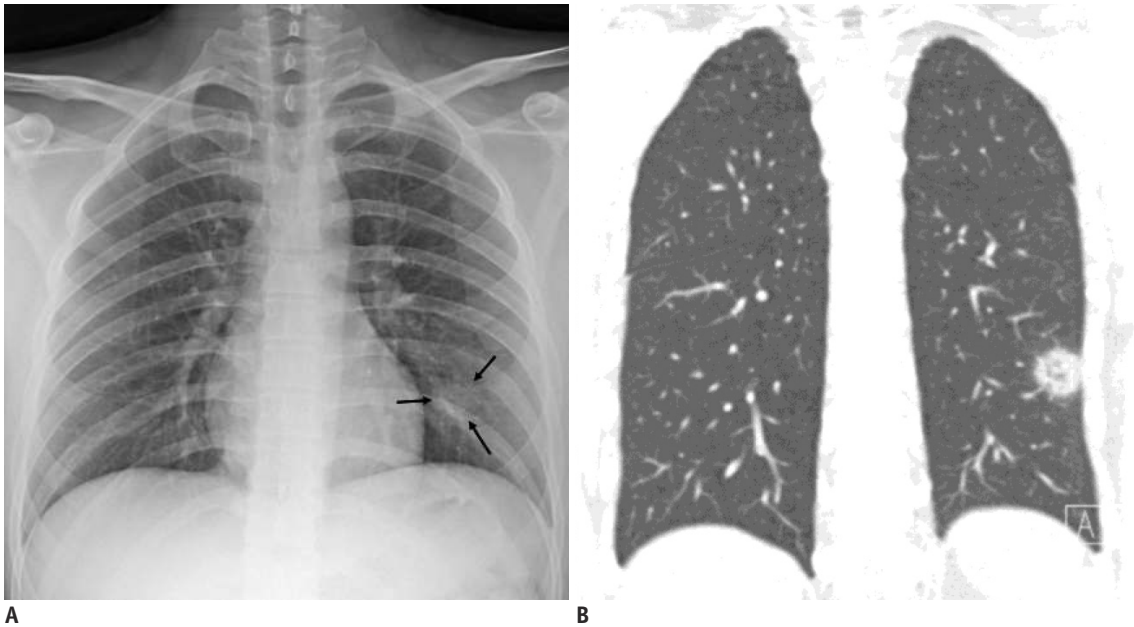

Fig. 3. Representative chest radiographic (A) and CT images (B) of COVID-19 pneumonia manifesting as single nodular lesion. A. Anteroposterior chest radiograph shows single nodular consolidation (arrows) in left lower lung zone. **B.** Coronal chest CT image taken on same day shows 2.3-cm ill-defined nodular lesion with reversed halo sign with thick rim in left lower lobe, abutting adjacent pleura.

https://doi.org/10.3348/kjr.2020.0132

Table 1. Per-Lesion Analysis of Chest Radiographic Findings

Chest Radiographic Findings	n (%)
Laterality	
Right lung	5 (50)
Left lung	5 (50)
Cephalocaudal distribution	
Upper lung zone	2 (20)
Middle lung zone	3 (30)
Lower lung zone	5 (50)
Central to peripheral distribution	
Central half	2 (20)
Peripheral half	6 (60)
Central and peripheral	2 (20)
Shape	
Patchy	9 (90)
Nodular	1 (10)
Density	
Consolidation	8 (80)
Ground-glass lesion	2 (20)

28% of the lesions had an air-bronchogram. Nodular lesions primarily manifested as pure GGO lesions (57%), followed by predominantly GGO lesions (32%) and predominantly solid lesions (11%). Nodular lesions were round (95%) and had ill-defined margins (75%). There were no cavities, micronodules, lesions with a tree-in-bud appearance, or pleural effusions. Compared to nodular lesions, patchy to confluent lesions were primarily distributed along the pleura (80% vs. 35%; $p < 0.001$) and more commonly involved the lower lobes (60% vs. 35%; $p = 0.040$) (Fig. 4A). The nodular lesions were primarily distributed along the bronchovascular bundles (59% vs. 28%; $p = 0.006$) (Fig. 4B) and tended to manifest as pure GGO lesions (57% vs. 35%; $p = 0.069$).

DISCUSSION

The outbreak of COVID-19 pneumonia has resulted in a global health emergency, similar to the outbreaks of severe

Table 2. Per-Lesion Analysis of Chest Computed Tomography Findings

Patchy to Confluent Lesions (n = 40)	n (%)	Nodular Lesions (n = 37)	n (%)
Density		Density	
Pure GGO	14 (35)	Pure ground-glass	21 (57)
Mixed GGO and consolidation	20 (50)	Part-solid	16 (43)
Consolidation	2 (5)	Solid	0 (0)
Crazy-paving appearance	4 (10)		-
Axial location		Axial location	
Central	1 (2)	Central	7 (19)
Peripheral	30 (75)	Peripheral	30 (81)
Central and peripheral	9 (23)		-
Anteroposterior location		Anteroposterior location	
Anterior	9 (23)	Anterior	13 (35)
Posterior	28 (70)	Posterior	24 (65)
Anterior and posterior	3 (7)		-
Shape		Shape	
Wedged	17 (42)	Round	35 (95)
Elongated	13 (33)	Elongated	2 (5)
Confluent	10 (25)		-
Margin		Margin	
Ill-defined	28 (70)	Ill-defined	28 (76)
Well-defined	12 (30)	Well-defined	9 (24)
Predilection for particular locations		Predilection for particular locations	
Lower lobe involvement	24 (60)	Lower lobe involvement	13 (35)
Pleural attachment	32 (80)	Pleural attachment	13 (35)
Bronchovascular bundle	11 (27)	Bronchovascular bundle	22 (59)
Internal characteristic findings		Internal characteristic findings	
Air-bronchogram	11 (28)	Air-bronchogram	5 (14)
	-	Reversed halo sign	1 (3)
	-	Cavity	0 (0)

GGO = ground-glass opacity

https://doi.org/10.3348/kjr.2020.0132

Korean Journal of Radiology
KJR

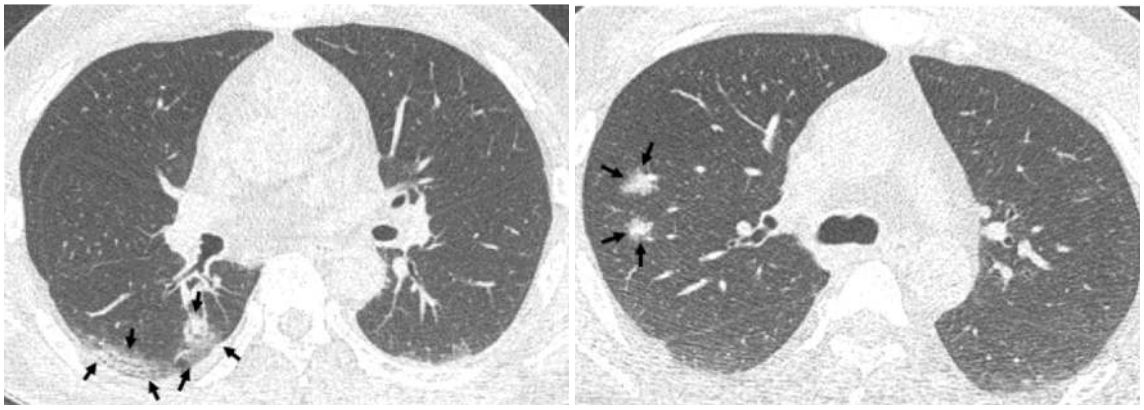

A B

Fig. 4. Representative CT images (A, B) of COVID-19 pneumonia manifesting as radiograph-negative multiple patchy to nodular mixed ground-glass opacities and consolidations. A. Axial chest CT image shows ill-defined mixed ground-glass opacities and consolidative lesions with patchy and elongated shape (arrows) touching pleura in superior segment of right lower lobe. **B.** Axial chest CT image shows ill-defined part-solid nodules (arrows; mixed ground-glass opacities and solid nodules) along bronchovascular bundles in posterior segment of right upper lobe.

acute respiratory syndrome (SARS) in 2003 and Middle East respiratory syndrome (MERS) in 2012, both of which were also caused by viruses belonging to the family *coronaviridae*. Indeed, COVID-19 pneumonia shows radiologic similarities to SARS and MERS pneumonia (10-14), with a predominance of bilateral GGO and consolidative lesions in the peripheral lung. Despite the similarities in CT findings, COVID-19 pneumonia seems radiologically milder than SARS and MERS pneumonia. The proportion of patients with abnormal initial radiographic findings was 78.3–82.4% in SARS (15, 16) and 83.6% in MERS (17), but only 33% in our cases of COVID-19 pneumonia. GGO lesions on CT without any consolidation presented in 45% of our cases and in 45–67% of Chinese COVID-19 patients (4, 5), in 14–40% of MERS patients (10, 11), and in 50% of SARS patients (12).

The CT findings of COVID-19 pneumonia in Korea were generally consistent with those of COVID-19 pneumonia in China (4-6, 18). However, the proportion of predominantly consolidative lesions in Chinese patients was approximately 30% (4) to 60% (5), but the Korean patients did not have predominantly consolidative lesions. Furthermore, the proportion of chest radiographic abnormalities was 60% in Chinese COVID-19 patients (19), but 33% in Korean patients. Considering these radiologic observations and the lack of deaths from COVID-19 in Korea, Korean patients seem to experience a milder disease course than Chinese patients.

Interestingly, we observed a reversed halo sign in one patient (Fig. 3B), and a few similar cases have been reported in recent reports (19-21). The reversed halo sign was first regarded as specific for cryptogenic organizing pneumonia, and it can be seen in various infectious diseases, including angioinvasive pulmonary aspergillosis or mucormycosis, paracoccidioidomycosis, *pneumocystis jiroveci* pneumonia, and tuberculosis (22). This sign might reflect an organizing pneumonia pattern in COVID-19 pneumonia (21).

A few limitations exist in this study. First, the number of included patients was small, and the included patients only accounted for approximately one-third of all 29 identified patients of COVID-19 in Korea as of February 16, 2020. Including more patients would enable a more comprehensive description of the radiologic findings of COVID-19. However, we weighed this consideration against the importance of urgent reporting. Second, we focused on baseline CT findings that clinicians and radiologists first encountered, rather than findings from follow-up CT scans, as follow-up CT scans were performed in few patients. Third, we minimized the clinical information of the patients, as a substantial proportion of the included patients were receiving inpatient treatment at the time of the analysis.

In conclusion, COVID-19 pneumonia in Korea generally manifested as pure GGO to mixed GGO and consolidative lesions in the bilateral peripheral posterior lungs. The shape of the lesions was typically ill-defined and patchy to confluent, or nodular. Patchy to confluent lesions were primarily distributed along the pleura, whereas nodular lesions were mainly distributed along the bronchovascular bundles. Most of the pulmonary lesions were ambiguous on chest radiographs. Clinicians and radiologists should become familiar with the CT findings of COVID-19 and the

 https://doi.org/10.3348/kjr.2020.0132

limitations of chest radiographs in evaluating pneumonia to manage the COVID-19 outbreak.

Conflicts of Interest

The authors have no potential conflicts of interest to disclose.

Acknowledgments

The authors would like to acknowledge Andrew Dombrowski, PhD (Compecs, Inc.) for his assistance in improving the use of English in this manuscript.

ORCID iD

Soon Ho Yoon
https://orcid.org/0000-0002-3700-0165

REFERENCES

1. Zhu N, Zhang D, Wang W, Li X, Yang B, Song J, et al.; China Novel Coronavirus Investigating and Research Team. A novel Coronavirus from patients with pneumonia in China, 2019. *N Engl J Med* 2020;382:727-733
2. Li Q, Guan X, Wu P, Wang X, Zhou L, Tong Y, et al. Early transmission dynamics in Wuhan, China, of novel Coronavirus-infected pneumonia. *N Engl J Med* 2020 Jan 29 [Epub]. https://doi.org/10.1056/NEJMoa2001316
3. Coronavirus disease 2019 (COVID-19) situation report–27. World Health Organization Web site. https://www.who.int/docs/default-source/coronaviruse/situation-reports/20200216-sitrep-27-covid-19.pdf?sfvrsn=78c0eb78_2. Published February 17, 2020. Accessed February 17, 2020
4. Chung M, Bernheim A, Mei X, Zhang N, Huang M, Zeng X, et al. CT imaging features of 2019 novel Coronavirus (2019-nCoV). *Radiology* 2020 Feb 4 [Epub]. https://doi.org/10.1148/radiol.2020200230
5. Song F, Shi N, Shan F, Zhang Z, Shen J, Lu H, et al. Emerging coronavirus 2019-nCoV pneumonia. *Radiology* 2020 Feb 6 [Epub]. https://doi.org/10.1148/radiol.2020200274
6. Pan F, Ye T, Sun P, Gui S, Liang B, Li L, et al. Time course of lung changes on chest CT during recovery from 2019 novel Coronavirus (COVID-19) pneumonia. *Radiology* 2020 Feb 13 [Epub]. https://doi.org/10.1148/radiol.2020200370
7. Kim JY, Choe PG, Oh Y, Oh KJ, Kim J, Park SJ, et al. The first case of 2019 novel Coronavirus pneumonia imported into Korea from Wuhan, China: implication for infection prevention and control measures. *J Korean Med Sci* 2020;35:e61
8. Taylor E, Haven K, Reed P, Bissielo A, Harvey D, McArthur C, et al.; SHIVERS Investigation Team. A chest radiograph scoring system in patients with severe acute respiratory infection: a validation study. *BMC Med Imaging* 2015;15:61
9. Hansell DM, Bankier AA, MacMahon H, McLoud TC, Müller NL, Remy J. Fleischner Society: glossary of terms for thoracic imaging. *Radiology* 2008;246:697-722
10. Ajlan AM, Ahyad RA, Jamjoom LG, Alharthy A, Madani TA. Middle East respiratory syndrome Coronavirus (MERS-CoV) infection: chest CT findings. *AJR Am J Roentgenol* 2014;203:782-787
11. Das KM, Lee EY, Enani MA, AlJawder SE, Singh R, Bashir S, et al. CT correlation with outcomes in 15 patients with acute Middle East respiratory syndrome coronavirus. *AJR Am J Roentgenol* 2015;204:736-742
12. Wong KT, Antonio GE, Hui DS, Lee N, Yuen EH, Wu A, et al. Thin-section CT of severe acute respiratory syndrome: evaluation of 73 patients exposed to or with the disease. *Radiology* 2003;228:395-400
13. Choi WJ, Lee KN, Kang EJ, Lee H. Middle East respiratory syndrome-Coronavirus infection: a case report of serial computed tomographic findings in a young male patient. *Korean J Radiol* 2016;17:166-170
14. Wan YL, Tsay PK, Cheung YC, Chiang PC, Wang CH, Tsai YH, et al. A correlation between the severity of lung lesions on radiographs and clinical findings in patients with severe acute respiratory syndrome. *Korean J Radiol* 2007;8:466-474
15. Antonio GE, Ooi CG, Wong KT, Tsui EL, Wong JS, Sy AN, et al. Radiographic-clinical correlation in severe acute respiratory syndrome: study of 1373 patients in Hong Kong. *Radiology* 2005;237:1081-1090
16. Wong KT, Antonio GE, Hui DS, Lee N, Yuen EH, Wu A, et al. Severe acute respiratory syndrome: radiographic appearances and pattern of progression in 138 patients. *Radiology* 2003;228:401-406
17. Das KM, Lee EY, Al Jawder SE, Enani MA, Singh R, Skakni L, et al. Acute Middle East respiratory syndrome Coronavirus: temporal lung changes observed on the chest radiographs of 55 patients. *AJR Am J Roentgenol* 2015;205:W267-W274
18. Lin X, Gong Z, Xiao Z, Xiong J, Fan B, Liu J. Novel Coronavirus pneumonia outbreak in 2019: computed tomographic findings in two cases. *Korean J Radiol* 2020 Feb 11 [Epub]. https://doi.org/10.3348/kjr.2020.0078
19. Ng MY, Lee EYP, Yang J, Yang F, Li X, Wang H, et al. Imaging profile of the COVID-19 infection: radiologic findings and literature review. *Radiology: Cardiothoracic Imaging* 2020;2:e200034
20. Fang Y, Zhang H, Xu Y, Xie J, Pang P, Ji W. CT manifestations of two cases of 2019 novel Coronavirus (2019-nCoV) pneumonia. *Radiology* 2020 Feb 7 [Epub]. https://doi.org/10.1148/radiol.2020200280
21. Kong W, Agarwal PP. Chest imaging appearance of COVID-19 infection. *Radiology: Cardiothoracic Imaging* 2020;2:e200028
22. Godoy MC, Viswanathan C, Marchiori E, Truong MT, Benveniste MF, Rossi S, et al. The reversed halo sign: update and differential diagnosis. *Br J Radiol* 2012;85:1226-1235